Research Square

Preprints are preliminary reports that have not undergone peer review.
They should not be considered conclusive, used to inform clinical practice,
or referenced by the media as validated information.

Synthesis and performance evaluation of hydrophobic association polymer by asymmetric double-tail chain hydrophobic associating monomer for fracturing fluids

wenfeng jia

jiawf@iccas.ac.cn

China University of Petroleum (Beijing)

Yuqi Chen

China University of Petroleum (Beijing)

junwen wu

Sinopec Exploration and Development Research Institute

Research Article

Keywords: Hydrophobic associative polymer, Water-based fracturing fluid, Polymer thickener, molecular dynamics simulation, Temperature and salt resistant

Posted Date: February 27th, 2026

DOI: https://doi.org/10.21203/rs.3.rs-8582478/v1

License: This work is licensed under a Creative Commons Attribution 4.0 International License.
Read Full License

Additional Declarations: No competing interests reported.

Synthesis and performance evaluation of hydrophobic association polymer by asymmetric double-tail chain hydrophobic associating monomer for fracturing fluids

Wenfeng Jia[a*], Yuqi Chen[a], Junwen Wu[b]

a) State Key Laboratory of Petroleum Resources and Engineering, China University of Petroleum (Beijing), Beijing, China. 102249；

b) Sinopec Exploration and Development Research Institute, Beijing, China 100083

Corresponding author: Wenfeng Jia

Email Address of the Corresponding Author: jiawf@iccas.ac.cn

Abstract

To address the challenges of conventional polymer fracturing fluids in hydraulic fracturing, including poor temperature-salt resistance, incomplete gel-breaking, and high production costs, this study designed and synthesized a novel hydrophobically associating polymer (AHAP). The molecular structure of the synthesized product was confirmed through FTIR analysis and ^{1}H-NMR characterization. Systematic investigations were conducted on the water solubility, thickening capacity, and temperature-salt tolerance of AHAP polymers. The self-assembly behavior of polymer chains was studied using the molecular dynamics simulation method, revealing the

interaction mechanism between polymer chains at the molecular level. Under high-temperature and high-salinity conditions, AHAP demonstrated markedly superior viscosity retention compared to HPAM. Rheological analysis showed that increasing polymer concentration delayed the crossover point of storage modulus (G') and loss modulus (G") in stress sweep tests while advancing it in frequency sweep tests, indicating excellent viscoelastic properties and proppant-carrying capacity.

Key Words: Hydrophobic associative polymer; Water-based fracturing fluid; Polymer thickener; molecular dynamics simulation; Temperature and salt resistant

1. Introduction

The investigation of low-permeability reservoirs holds significant importance both theoretically and technically. However, such reservoirs present substantial challenges including high extraction costs, technical complexities, and suboptimal production outcomes due to their inherent characteristics of small pore throats, low porosity, poor pore connectivity, and complex pore network structures[1-3]. Since its first implementation in 1947, hydraulic fracturing has become one of the most effective enhanced oil recovery methods, recognized for its operational simplicity, cost-effectiveness, and superior fracturing performance[4]. Water-based fracturing fluids, currently the most widely used fracturing systems worldwide, offer distinct advantages including broad applicability, excellent proppant-carrying capacity, low cost, minimal fluid loss, and operational flexibility[5]. As the core component of water-based fracturing systems, the molecular structure of thickeners directly determines the

57 performance characteristics of fracturing fluids[6, 7]. While polyacrylamide (PAM) has
58 been widely employed, the increasing field requirements for high-temperature and salt-
59 tolerant fracturing fluids have exposed the limitations of conventional polymers.
60 Consequently, hydrophobically associating polymers (HAPs) have emerged as a
61 prominent research focus due to their exceptional temperature and salt resistance
62 properties[8-11].

63 Hydrophobically associating polymers (HAPs) are functional polymeric materials
64 incorporating a small number of hydrophobic groups into hydrophilic polymer
65 backbones. Although exhibiting lower molecular weights compared to conventional
66 linear polyacrylamide-based polymers, HAPs can form dynamic reversible cross-linked
67 network structures through the unique hydrophobic association of their pendant
68 groups[12, 13]. While both HAPs and traditional water-soluble polymers can establish
69 network structures at sufficient concentrations, their formation mechanisms differ
70 fundamentally: HAP networks originate from hydrophobic associations, whereas
71 conventional systems rely solely on physical chain entanglements[14]. The hydrophobic
72 association mechanism generates substantially higher energy states compared to
73 physical entanglement, with this energy hierarchy difference enabling HAP systems to
74 demonstrate superior apparent viscosity and structural strength[15].

Hydrophobic groups in current applications can be classified into three categories based on structural configurations: aromatic hydrophobic monomers (containing benzene rings), fluorinated alkyl hydrophobic monomers, and alkyl chain hydrophobic monomers. The rigid benzene ring in aromatic hydrophobic monomers effectively suppresses molecular chain bending, while its planar conjugated structure induces van der Waals forces to establish robust association networks. This dual mechanism (steric hindrance suppression - intermolecular interactions) significantly enhances the viscoelasticity of polymer solutions, demonstrating exceptional thickening performance. In fluorinated alkyl monomers, the strong electronegativity of fluorine atoms endows fluorocarbon chains with extraordinary hydrophobic association capability, reducing their critical association concentration (CAC) compared to hydrocarbon chains of equivalent length[16]. However, excessive fluorine content induces excessive hydrophobicity in polymer chains, leading to severe phase separation and compromised solubility. Moreover, the high production costs of fluorinated alkyl monomers substantially limit their industrial scalability. Although alkyl chain hydrophobic monomers exhibit weaker association strength than the aforementioned categories, their molecular design flexibility enables performance optimization through chain length modulation (C_{12}-C_{18})[17, 18]. Crucially, these monomers possess well-established industrial synthesis pathways and significant cost advantages, making them

94 irreplaceable in large-scale oilfield chemical applications such as fracturing fluids and
95 enhanced oil recovery agents. From a structural topology perspective, hydrophobically
96 associating polymers can be further categorized into two types based on hydrophobic
97 group positioning: graft-type (side-chain functionalized) and block-type (terminal
98 functionalized). In graft-type polymers, randomly distributed hydrophobic groups
99 along the backbone form isolated microdomains through intramolecular associations at
100 subcritical concentrations (C < CAC). Upon exceeding CAC, intermolecular
101 associations between these hydrophobic groups create dynamic cross-linked networks,
102 resulting in concentration-dependent viscosity enhancement[19, 20]. For block-type
103 polymers, terminal-positioned hydrophobic groups exhibit reduced steric hindrance,
104 significantly increasing intermolecular association probabilities[21]. As polymer chain
105 length increases, the growing number of intermolecular association sites strengthens
106 network cross-linking intensity, manifesting as substantial viscosity elevation in
107 macroscopic properties[22].
108 With the progression of reservoir development, polymer molecular chains become
109 disrupted under high-temperature and high-salinity conditions, leading to viscosity
110 degradation in solutions[23-25]. Elevated temperatures also induce hydrolysis of amide
111 groups in polyacrylamide into carboxylate groups, thereby reducing the polymer`s salt
112 tolerance[26, 27]. Furthermore, during operational processes, intensive mechanical

113 shearing damages polymer molecular structures through chain scission, compromising
114 viscoelastic properties and causing viscosity deterioration that ultimately impairs
115 application performance[28].
116 To address these challenges, this study employs a novel anionic asymmetric double-tail
117 chain hydrophobic monomer: ammonium 1-allyloxy-3-(4-nonylphenol)-2-propanol
118 polyoxyethylene (10) ether sulfate (DNS-86). This monomer demonstrates multiple
119 advantages: (1) The hydrophilic ethylene oxide (EO) chains enhance polymer
120 viscoelasticity without compromising association capabilities[29]; (2) The alkylbenzene
121 structure increases molecular chain rigidity, suppressing metal ion-induced chain
122 contraction and coiling while reinforcing polymer stability[30, 31]. A novel
123 hydrophobically associating polymer (AHAP) was synthesized via aqueous free radical
124 copolymerization of DNS-86 with acrylamide (AM) and 2-acrylamido-2-
125 methylpropanesulfonic acid (AMPS). This polymerization method offers operational
126 simplicity, minimal environmental impact, and direct copolymerization of ionic
127 hydrophobic monomers with water-soluble counterparts in aqueous phase without
128 requiring additional purification[32]. Comprehensive evaluations were conducted on
129 AHAP's viscosity-enhancing capability, solubility, and temperature-salt resistance. To
130 further investigate the mechanisms at the molecular level, we conducted molecular
131 dynamics simulations to study the self-assembly behavior of polymers.

2. Materials and experiment

2.1 Materials

Acrylamide (AM) and 2-acrylamido-2-methylpropanesulfonic acid (AMPS) were purchased from Shanghai Macklin Biochemical Technology Co., Ltd. Ammonium 1-allyloxy-3-(4-nonylphenol)-2-propanol polyoxyethylene (10) ether sulfate (DNS-86), as shown in fig. 1 was obtained from Guangzhou Shuangjian Trading Co., Ltd. Sodium hydroxide (NaOH), sodium chloride (NaCl), sodium sulfate (Na_2SO_4), sodium bicarbonate ($NaHCO_3$), calcium chloride ($CaCl_2$), magnesium chloride hexahydrate ($MgCl_2 \cdot 6H_2O$), sodium bisulfite ($NaHSO_3$), and potassium chloride (KCl) were supplied by Sinopharm Chemical Reagent Co., Ltd. Initiators including ammonium persulfate ($(NH_4)_2S_2O_8$) and 2,2'-azobis[2-(2-imidazolin-2-yl)propane] dihydrochloride (V-044) were acquired from Shanghai Titan Scientific Co., Ltd. These drugs are analytical grade and can be used directly without further processing. Deionized water was prepared in-house using a laboratory purification system.

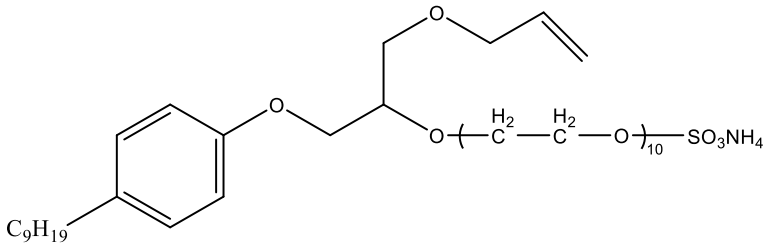


Fig. 1. Hydrophobic monomers: DNS-86

2.2 Synthesis of polymer AHAP

The synthetic route of polymer AHAP is illustrated in Fig. 2. The detailed procedure is described as follows:

Acrylamide (AM) and 2-acrylamido-2-methylpropanesulfonic acid (AMPS) at a mass ratio of 8:2 was dissolved in the water, followed by the addition of 1.2 wt.% hydrophobic monomer DNS-86. After complete dissolution, a 10% NaOH solution was added dropwise to adjust the pH to 8. The monomer solution was equilibrated to 25°C. Azo-initiator V-044 (0.0020 wt.%) was added to the solution under continuous N_2 purging. After 25 min, a redox initiator system comprising $(NH_4)_2S_2O_8$ and $NaHSO_3$ (each 0.0020 wt.%) was introduced while maintaining N_2 flow. After 6 h of reaction, the resulting gel was granulated using a mechanical grinder. The granules were uniformly mixed with NaOH (20% hydrolysis degree), and hydrolyzed at 80 °C for 2 h. Following hydrolysis, the product was dried at 60 °C for 8 h, pulverized into powder, and sieved through a 60-mesh screen to obtain the final white powdery AHAP thickener.

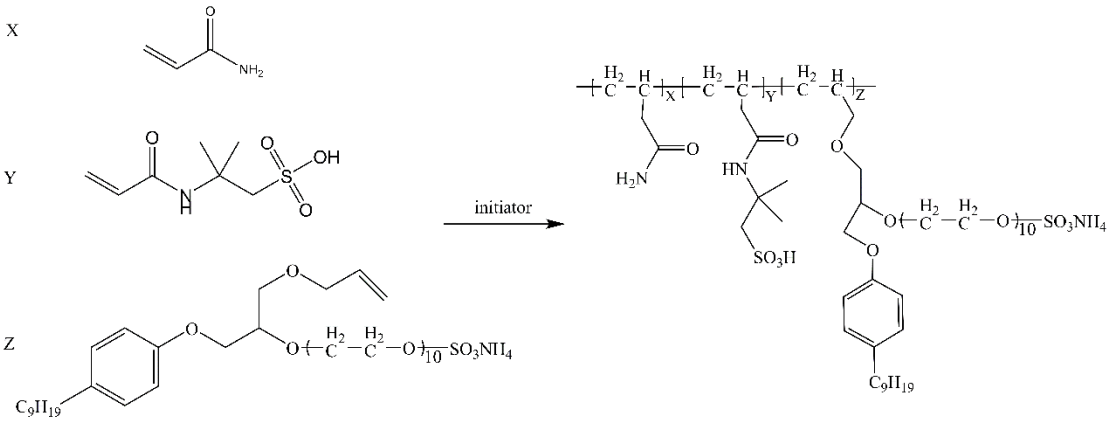


Fig. 2. The synthesis route of polymer AHAP

2.3 Experiment

2.3.1 FT-IR

The functional groups of AHAP within the wavenumber range of 4000-300 cm^{-1} were characterized using a Fourier transform infrared (FTIR) spectrometer (Nicolet iS50, Thermo Fisher Scientific Inc., USA). Prior to testing, the polymer powder was ground into a fine powder, thoroughly dried, and subsequently homogenized with pure potassium bromide (KBr) at a mass ratio of 1:100, followed by pellet formation under controlled pressure.

2.3.2 ^{1}H NMR

The structural characterization of AHAP was conducted via ^{1}H nuclear magnetic resonance (NMR) spectroscopy using a liquid-state NMR spectrometer (Ascend 500M, Bruker (Beijing) Technology Co., Ltd., China). Prior to analysis, the samples were dissolved in deuterium oxide (D_2O) as the deuterated solvent for spectral acquisition.

2.3.3 Molecular weight

The molecular weight determination of the polymer was performed using an Ubbelohde viscometer through the stepwise dilution method. Viscosity-concentration plots were systematically constructed, followed by molecular weight calculations based on intrinsic viscosity extrapolation.

2.3.4 Thickening performance

The rheological evaluation of polymer-containing solutions was conducted using a six-speed rotational viscometer (Model ZNN-D6S, Qingdao Hengtaida Electromechanical Equipment Co., Ltd., China). Systematic viscosity measurements were performed across a concentration gradient of 0.01-0.50 wt.% polymer under controlled shear conditions (170 s^{-1}) at 25 °C, followed by construction of the viscosity-concentration profile through graphical analysis.

2.3.5 Water solubility

The time-dependent viscosity evolution of 0.5 wt.% AHAP and HPAM solutions was investigated using a six-speed rotational viscometer (Model ZNN-D6S, Qingdao Hengtaida Electromechanical Equipment Co., Ltd., China) under standardized rheometric conditions (shear rate: 170 s^{-1}; temperature: 25 °C). Viscosity growth kinetics were quantitatively recorded from t = 1 min post-solubilization, with

197 subsequent construction of viscosity-temporal profiles through systematic chrono-
198 rheological analysis.

199 2.3.6 Temperature resistance

200 The viscosity changes of 0.5% AHAP and HPAM solutions were measured using a six-
201 speed rotational viscometer (Model ZNN-D6S, Qingdao Hengtaida Electromechanical
202 Equipment Co., Ltd.) under a shear rate of 170 s^{-1} at 25 °C, with temperature variations
203 from 25 °C to 90 °C.

204 2.3.7 Salt resistance

205 The ionic responsiveness of 0.5 wt.% AHAP and HPAM solutions was systematically
206 evaluated through multi-electrolyte rheological screening. Polymer solutions were
207 formulated with seven salt types (NaCl, Na_2SO_4, $NaHCO_3$, $CaCl_2$, $MgCl_2 \cdot 6H_2O$,
208 $NaHSO_4$, and KCl) across gradient concentrations using a six-speed rotational
209 viscometer (Model ZNN-D6S, Qingdao Hengtaida Electromechanical Equipment Co.,
210 Ltd., China). Post-hydration viscosity measurements under standardized shear (170 s^{-1})
211 and thermal (25 °C) conditions enabled construction of comparative viscosity-salinity
212 profiles, elucidating polymer-salt specificity through cationic/anionic valency-
213 controlled analysis.

2.3.8 Rheological performance evaluation

The rheological properties of fracturing fluid can reflect the performance of polymer thickener products. Prepare 0.6%, 0.5%, 0.4%, 0.3% polymer AHAP solution to ensure that it is completely dissolved. The rheological properties of polymer fracturing fluids, including temperature and shear resistance and viscoelasticity, were determined using a Harker Rheometer (MARSIII, Haake, Germany).

2.3.9 Sand carrying performance

The proppant-carrying capacity of fracturing fluids directly determines the success of hydraulic fracturing operations. The static settling velocity of solid-phase proppants in AHAP polymer-based fracturing fluids was observed to evaluate their sand suspension performance. Polymer fracturing fluids were prepared with AHAP concentrations of 0.5%, 0.4%, and 0.3%. Each fluid was mixed with 20% (by weight) of 20-40 mesh quartz sand, allowed to stand at ambient temperature, and monitored for static settling by recording the initial sand position and observing sedimentation behavior.

2.3.10 Rubber breaking property

The gel-breaking rate and completeness of polymer fracturing fluids critically determine the success of fracturing operations. AHAP polymer solutions (0.1-0.5%) and 0.5% HPAM solution were prepared with gradient concentrations of ammonium persulfate breaker. These mixtures were incubated in an 80°C constant-temperature

water bath to monitor gel-breaking progress and record the gel-breaking time. Post-breaking solutions were settled to room temperature for subsequent surface tension and interfacial tension measurements.

2.4 Simulation details

2.4.1 Simulation method

All MD simulations were conducted using GROMACS 2024.03 code and OPLS-AA plus SPCE force fields which are successfully described this kind of system[33, 34]. We optimized the molecule structures used in the simulation system at the B3LYP/def2TZVP level and obtained the RESP2 atomic charges by Multiwfn software[35, 36].

The long-range electrostatic interaction was calculated by Partial Mesh Ewald (PME) [37]. All bonds were constrained by the LINCS algorithm[38]. The cut-off radius of non-bond interaction was selected as 1.2 nm. To ensure the accuracy of simulation results, the methods of periodic calculation were used to simulate each system. Temperature was set at 300 K, which was achieved by Berendsen hot bath method[39]. The pressure was controlled with a Parrinello-Rahman barostat with a time constant of 2 ps for equilibration and production[40]. Time step of 2 fs was set for the simulations，and The production run was carried out with an NPT ensemble during 400 ns. The coordinates

were saved at 10 ps intervals. Trajectories are analyzed using GROMACS tools. The simulation trajectory can be observed by visual software VMD 1.9.3[41].

2.4.2 Simulation system

We constructed a polymer model consisting of 60 monomers, with 3 functional monomers[42]. A box of 13.6 x 13.6 x 13.6 nm^3 was generated using the PACKMOL package[43]. The simulation system contains different quantities of polymer chains, which are used to simulate the interactions between polymers.

3 Results and discussion

3.1 FT-IR spectra analysis

The FT-IR spectrum of the AHAP polymer is shown in Fig. 3. Stretching vibration peaks of unsaturated C-H bonds and saturated C-H bonds can be observed at 3190.2 cm^{-1} and 2929.5 cm^{-1}, respectively. Stretching vibration peaks of N-H and C=O bonds in the -$CONH_2$ group of AM are observed at 3339.1 cm^{-1} and 1659 cm^{-1}. Stretching vibration peaks of the -SO_3H group in AMPS are observed at 1193.6 cm^{-1}, 1049.3 cm^{-1}, and 495.5 cm^{-1}. The aromatic ring skeletal vibration absorption peak of DNS-86 is observed at 1556.6 cm^{-1}, and the stretching vibration absorption peak of the C-O-C bond in DNS-86 is observed at 1319.2 cm^{-1}. Deformation vibration absorption peaks of the -CH_3 group in AMPS and DNS-86 are observed at 1449.5 cm^{-1} and 1403 cm^{-1}. In summary, the absorption peaks in the infrared spectrum correspond to the functional

groups in the synthesized target polymer structure, confirming that the experimentally synthesized polymer is the desired product.

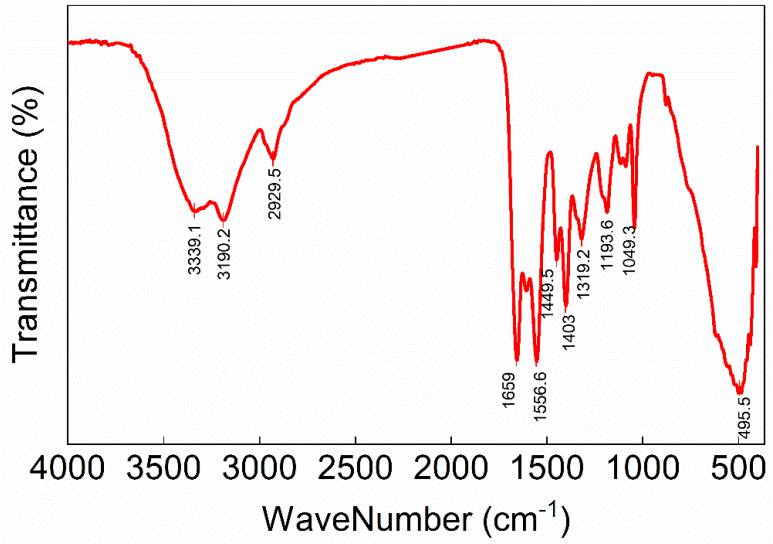


Fig. 3. FT-IR spectra of polymer AHAP

3.2 ^{1}H NMR analysis

The ^{1}H-NMR analysis spectrum of polymer AHAP is shown in Fig. 4. At δ = 1.49 ppm and 2.20 ppm, the chemical shifts of H on methylene (-CH_2) and methine (-CH) in the polymer backbone are observed, corresponding to the numbers 1, 3, 5 and 2, 4, 6 respectively. At δ = 1.49 ppm and 3.52 ppm, the chemical shifts of H on methyl (-CH_3) and methylene (-CH_2) in the AMPS side chain are detected, corresponding to the numbers 7 and 8 respectively. At δ = 3.50 ppm, the chemical shift of H on the methylene (-CH_2) connected to the ether bond in DNS-86 is found, corresponding to the numbers 9 and 10. At δ = 3.79 ppm and 3.81 ppm, the chemical shifts of H on the methine (-CH) connected to the ether bond and the methylene (-CH_2) connected to the side chain in

DNS - 86 are measured, corresponding to the numbers 11 and 12. At δ = 1.19 ppm and 1.07 ppm, the chemical shifts of H on the methylene (-CH_2) and methyl (-CH_3) connected to the benzene ring in the side chain of DNS-86 are identified, corresponding to the numbers 13 and 14. At δ = 3.65 ppm, the chemical shift of H on the EO chain in DNS-86 is determined, corresponding to the numbers 15 and 16. In conclusion, according to the ^{1}H-NMR analysis of the polymer, the polymer product exhibits the corresponding chemical shifts. Therefore, it can be confirmed that the polymer synthesized in the experiment is the target polymer product.

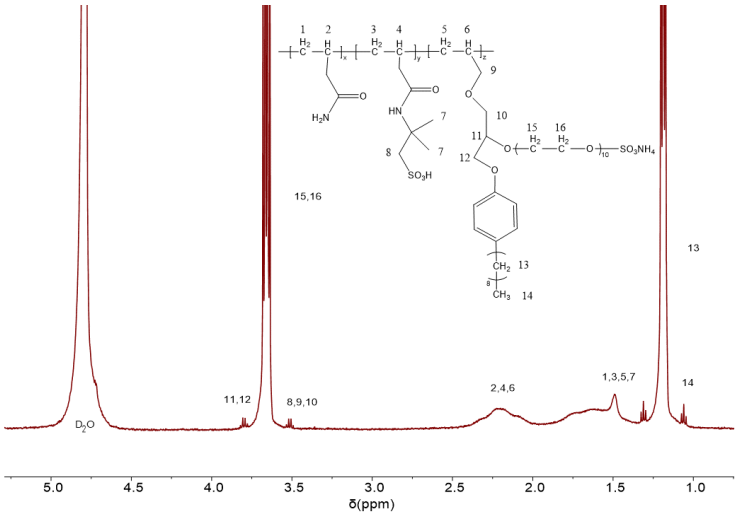


Fig. 4. The ^{1}H NMR spectra of polymer AHAP

3.3 Molecular weight

The dilution method was used to carry out the experiment, and the experimental data were processed:

The relative viscosity of the polymer solution is calculated according to equation (1) :

298 $$\eta_r = t/t_0 \quad (1)$$

299 In the equation： η_r: relative viscosity; t: flow time of the polymer solution (s); t_0: Flow

300 time of the 1.00 mol/L sodium chloride (NaCl) solution (s).

301 The increased viscosity of polymer solution is calculated according to equation (2) :

302 $$\eta_{sp} = \frac{t-t_0}{t_0} = \eta_r - 1 \quad (2)$$

303 In the equation: η_{sp}: specific viscosity; t: flow time of the polymer solution (s); t_0: flow

304 time of the 1.00 mol/L sodium chloride (NaCl) solution (s).

305 Plot specific viscosity/concentration (η_{sp}/C_r) and reduced logarithmic viscosity ($\ln\eta_r/C_r$)

306 on the vertical axis, with relative concentration (C_r) on the horizontal axis (where C_r is

307 the ratio of the diluted sample concentration to the original concentration). Extrapolate

308 Cr to zero to determine the intercept H. If the intercepts of the two lines differ, use their

309 average as H.

310 The characteristic viscosity number of polymer solution is calculated according to

311 equation (3) :

312 $$[\eta] = H/c_0 \quad (3)$$

313 In the equation: [η]: intrinsic viscosity (dL/g); c_0: initial concentration of the polymer

314 solution (g/dL).

315 The relative molecular mass of the polymer is calculated according to equation (4) :

316 $$[\eta] = KM^{\alpha} \quad (4)$$

In the equation: [η] : intrinsic viscosity (dL/g); K and α: Empirical constants, K=3.73×10^{-4} dL/g and α=0.66.

Through calculations, the relationship between the specific viscosity/concentration (η_{sp}/C_r) and reduced logarithmic viscosity ($\ln\eta_r/C_r$) of the polymer sample versus the relative concentration (C_r) is shown in Fig. 5.

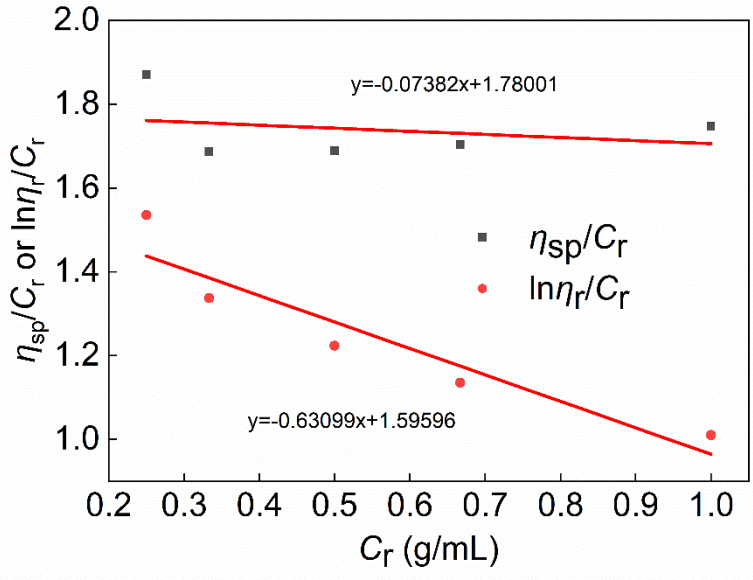


Fig. 5. Schematic diagram of polymer viscosity relationship

The intercept H of the polymer is 1.68799. Calculated from Equation (3), the intrinsic viscosity of the polymer is 16.8799 dL/g. Then, according to Equation (4), the molecular weight of the polymer is approximately 1.13×10^7 g/mol.

3.4 Thickening performance

The relationship between solution viscosity and polymer concentration for AHAP and HPAM is shown in Fig. 6. The viscosity of both polymer solutions increases with rising concentration. For HPAM, when the concentration reaches 0.131%, chain entanglement occurs, leading to a rapid viscosity increase. In contrast, AHAP exhibits a slow viscosity rise at concentrations below 0.085%. When the concentration falls within 0.085%–0.233% (the first critical association concentration), the apparent viscosity increases at an accelerated rate. Beyond 0.233% (the second critical association concentration), the apparent viscosity surges rapidly.

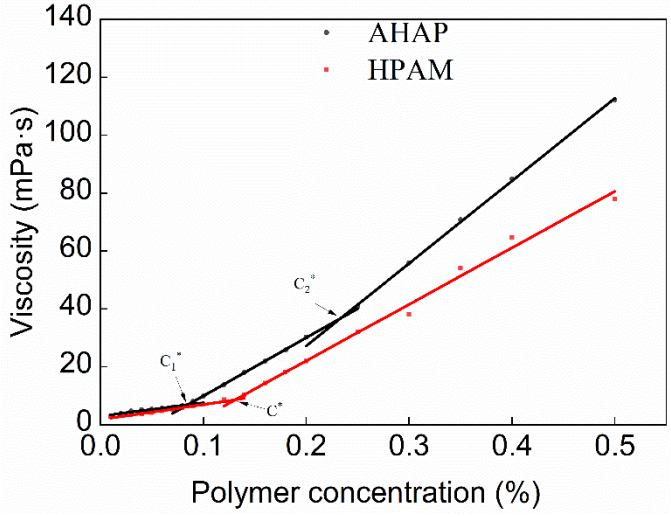


Fig. 6. Effect of polymer concentration on apparent viscosity of polymer solution

Unlike conventional hydrophobic monomers, the hydrophobic monomer DNS-86 features a long hydrophilic ethylene oxide (EO) chain and a short hydrophobic alkyl chain. This unique structure is responsible for the observed multiple critical association

concentrations, as illustrated in Figure. 7. When C < C_1*: At low polymer concentrations, intramolecular associations dominate. The alkyl chains form isolated microdomains via intramolecular interactions, while the highly hydrated EO chains remain extended without forming entangled structures, resulting in small hydrodynamic volumes and low solution viscosity. When C_1^*<C<C_2^*: The EO chains reach their entanglement concentration, leading to physical entanglement and the formation of a transient crosslinked network. The hydrodynamic volume of the polymer increases, causing a gradual rise in solution viscosity. When C>C_2^*: The hydrophobic groups on the polymer chains reach their critical association concentration. Intermolecular associations become dominant, and the synergistic effects of hydrophobic interactions and chain entanglement create a stable EO chain entanglement-hydrophobic association" crosslinked network, resulting in a sharp increase in solution viscosity.

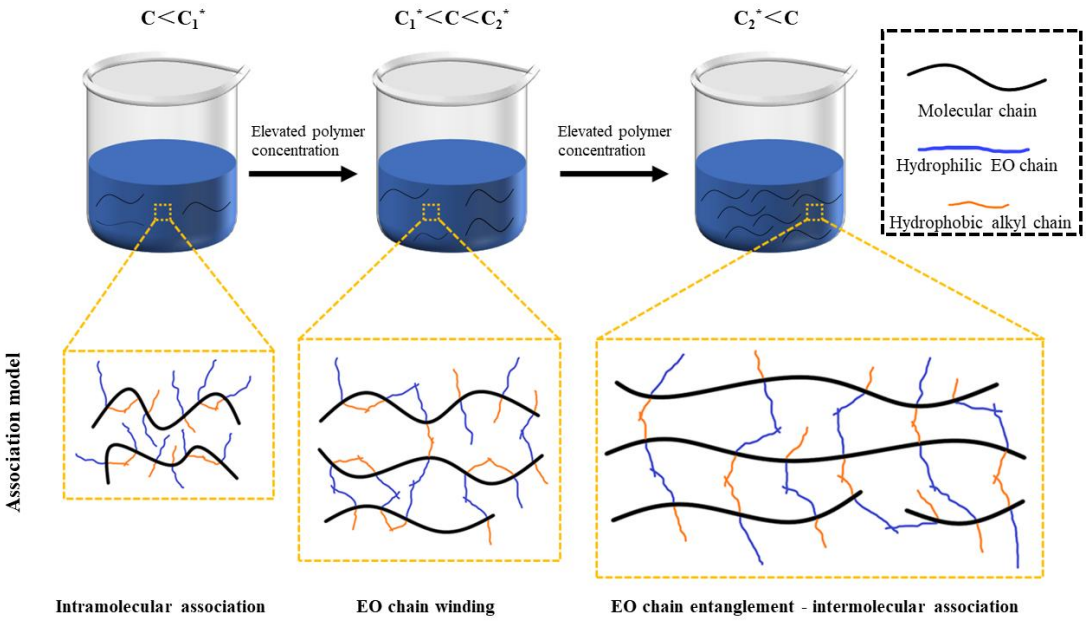


Fig.7. Schematic diagram of polymer multiple critical association concentration mechanism

The assembly behavior of one polymer chain and 15 polymer chains at room temperature was studied using the full-atom molecular dynamics simulation method. From Fig. 8. b) and c), it can be seen that after 400 ns of dynamic simulation, one polymer chain exhibited certain intramolecular aggregation behavior, indicating that the hydrophobic segments on the hydrophobic associating monomers have a significant impact on the swelling and dissolution of the polymer. From Fig. 8. d) and e), it can be seen that in the presence of 15 high-order polymer chains, intermolecular association occurred between AHAPs, and through intermolecular association, the viscoelastic properties were improved.

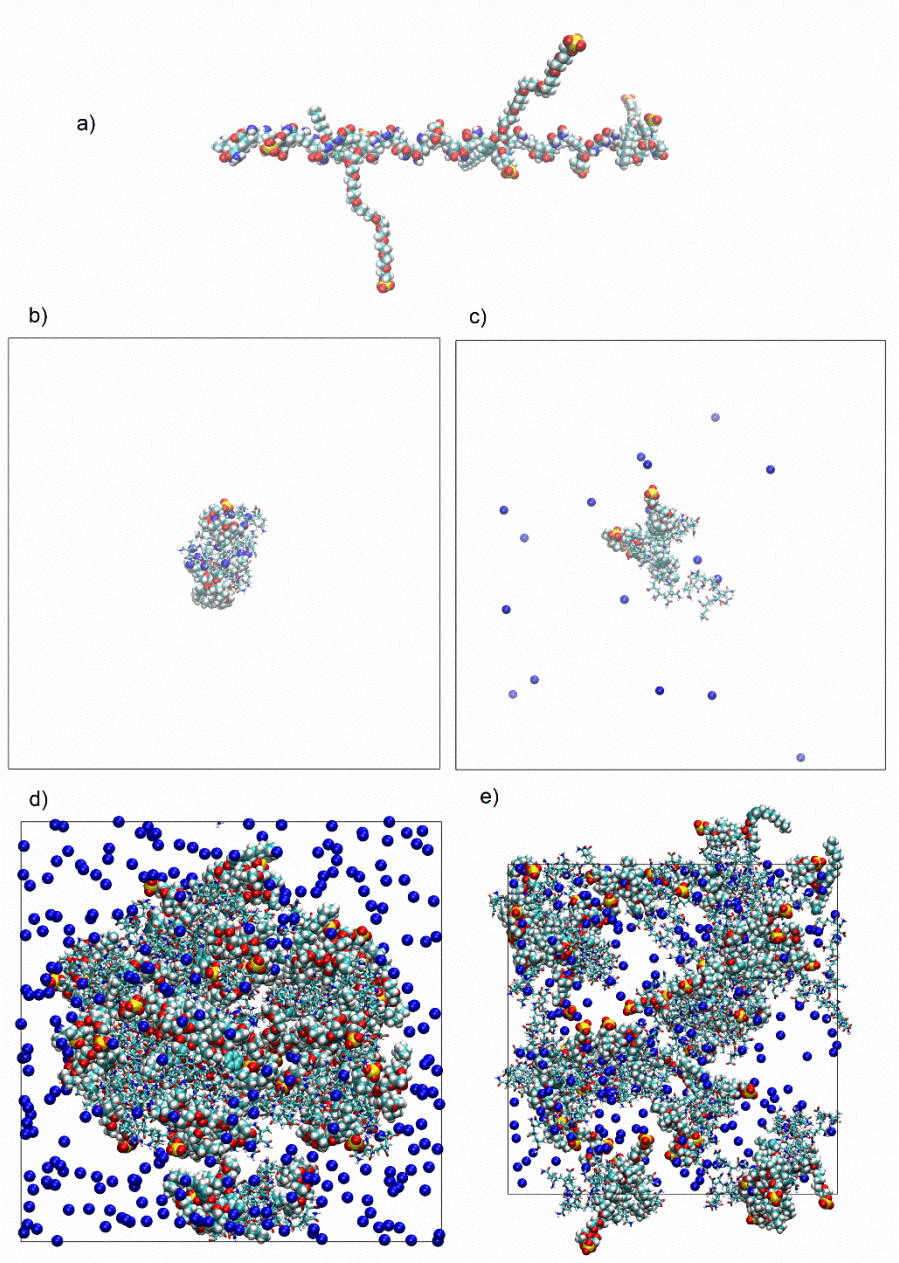


Fig.8. (a) Molecular models of AHAP. Colors for the atom scheme are N- blue, O-red, H-white, C-gray, and S-yellow, respectively. (b) and (d) The initial configurations of the simulation systems with 1 and 15 polymer, respectively. (c) and (4) The final configurations of the simulation systems with 1 and 15 polymer, respectively. In panels b, c, d, and e, the hydrophobic associating monomer

371 are shown in VDW mode, AM, AA, and, AMPS monmers are shown in Licorice mode, and the
372 colors for the atoms are N- blue, O-red, C-light blue, S-yellow, and H-white, respectively. The water
373 molecules are not shown for clarity.
374
375 From Fig. 9. a), it can be seen that under the conditions of one and 15 AHAP polymer
376 chains, the radius of gyration (Rg) changed significantly. Due to the intermolecular
377 association between polymer chains, the polymer chains elongated, Rg increased, and
378 thus the viscosity of the polymer solution significantly improved rapidly with
379 concentration. From Fig. 9. b), it can be seen that in the solution of 15 AHAP polymer
380 chains, there were multiple peaks between the hydrophobic associating monomers
381 DNS-86, proving that there are certain hydrophobic association effects both between
382 and within molecules.

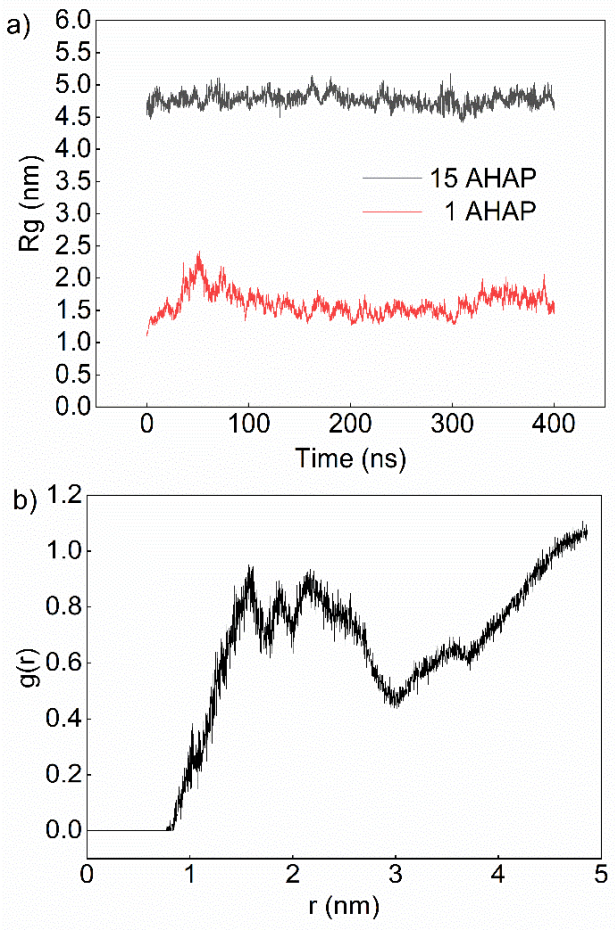


Fig. 9. (a) Rg under the conditions of one and 15 polymer molecules; (b) radial distribution functions (rdf) under the conditions 15 polymer molecules.

3.5 Water solubility

Compared to conventional polymers, hydrophobically associating polymers incorporate hydrophobic groups into their molecular chains. These groups form a unique three-dimensional crosslinked network through hydrophobic associations, endowing the polymers with enhanced performance. However, this also increases the

391 hydrophobicity of HAPs, negatively impacting their solubility and preventing rapid
392 dissolution in water.
393 Fig. 10. illustrates the relationship between solution viscosity and dissolution time for
394 0.5% AHAP and HPAM. The viscosity of both solutions increases with dissolution
395 time, stabilizing after 870 s for AHAP and 670 s for HPAM, with no significant changes
396 thereafter. Visual inspection confirmed no flocculation or undissolved aggregates,
397 indicating complete dissolution of the polymers.
398 The introduction of AMPS and the hydrophobic monomer DNS-86 enhances the
399 rigidity of the AHAP molecular chains, partially counteracting the reduced solubility
400 caused by increased hydrophobicity. While AHAP exhibits slightly slower dissolution
401 compared to HPAM, its shorter dissolution time (870 s) and superior thickening
402 capability still meet the requirements for on-site fracturing fluid operations. This
403 balance ensures AHAP remains practical for field applications despite its inherent
404 hydrophobic challenges.

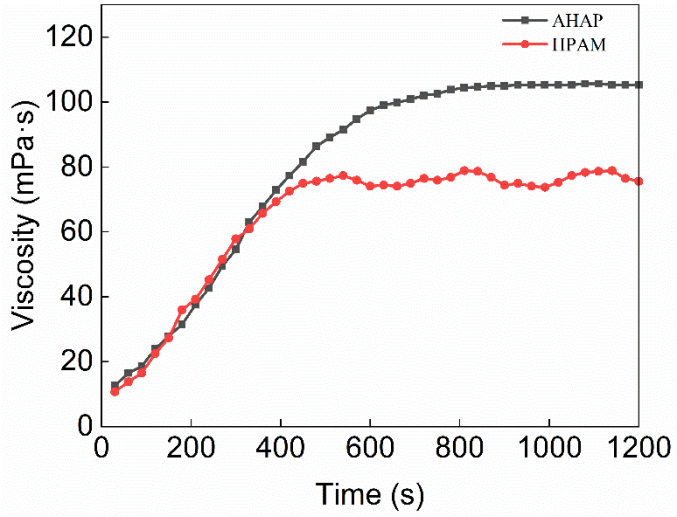


Fig. 10. Effect of dissolution time on apparent viscosity of polymer solution

3.6 Temperature resistance

The relationship between solution viscosity and temperature for 0.5% AHAP and HPAM is shown in Fig. 11. As temperature increases, the viscosity of both polymer solutions initially rises and then declines. When the temperature increases from 25°C to 30°C, the viscosity of the polymer solutions slightly increases. This is attributed to the rise in system entropy caused by higher temperatures, which promotes entanglement of ethylene oxide (EO) chains. Additionally, increased molecular motion at elevated temperatures drives hydrophobic groups on the polymer chains that were previously unassociated to form intermolecular associations, leading to a slight increase in apparent viscosity.

However, when the temperature exceeds 30°C, the viscosity gradually decreases. This occurs because further temperature increases enhance thermal perturbation effects,

causing the dissociation rate of hydrophobic associations to surpass the association rate. As a result, the hydrophobic interactions weaken, and viscosity declines. At 90°C, the viscosity of the HPAM solution drops significantly, indicating its limited thickening capability under high-temperature conditions. In contrast, the apparent viscosity of the AHAP solution remains at 69.3 mPa·s. This superior performance of AHAP is due to the bulky side groups in AMPS and DNS-86, which enhance the rigidity of the polymer chains, suppress hydrolysis of amide groups at high temperatures, and reduce thermal sensitivity. Furthermore, the introduction of DNS-86 provides hydrophobic associations that further improve the polymer's thermal stability. In summary, AHAP demonstrates excellent temperature resistance, making it more suitable for high-temperature applications compared to HPAM.

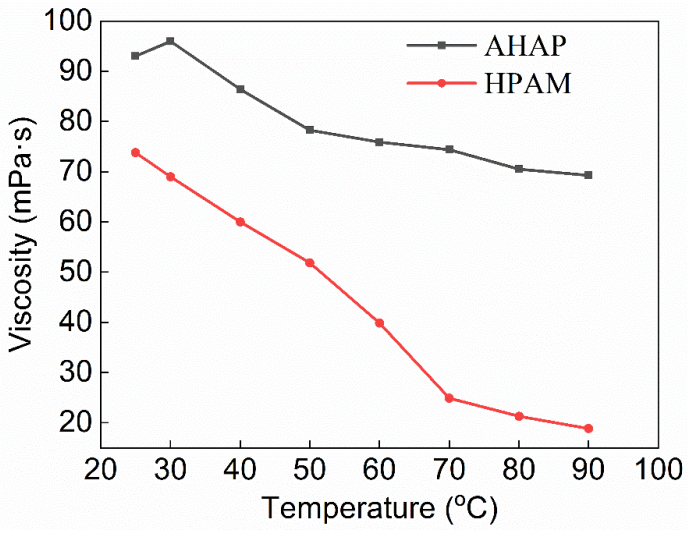


Fig. 11. Effect of temperature on the apparent viscosity of polymer solutions

3.7 Salt resistance

Fig. 12(a) and (b) show the effects of NaCl concentration on the viscosity and viscosity retention rate of polymer solutions. The viscosity of the polymer solutions gradually decreases with increasing NaCl concentration. When the NaCl concentration exceeds 5000 mg/L, the viscosity change of AHAP becomes less pronounced and gradually stabilizes. At a NaCl concentration of 7000 mg/L, the AHAP solution maintains a viscosity of 58.5 mPa·s, demonstrating a significantly higher viscosity retention rate compared to HPAM.

Fig. 12(c) and (d) illustrate the effects of $CaCl_2$ and simulated formation water (composition listed in Table 1) on polymer solution viscosity. The viscosity decreases gradually with increasing $CaCl_2$ concentration. Divalent metal cations exhibit a stronger impact on polymer solutions. At a $CaCl_2$ concentration of 2000 mg/L, the AHAP solution retains a viscosity of 44.4 mPa·s, outperforming HPAM in viscosity retention. This indicates that AHAP, relying on hydrophobic associations, maintains viscosity stability even under high $CaCl_2$ concentrations, showcasing superior salt tolerance over conventional polymers.

In simulated formation water, when the salinity exceeds 20000 mg/L, the viscosity retention rate of AHAP remains nearly constant with further increases in salinity. This

performance far exceeds that of HPAM in high-salinity complex brines, further confirming AHAP's exceptional salt resistance.

Table 1 Simulated formation water composition

Na^+	Ca^{2+}	Mg^{2+}	K^+	SO_4^{2-}	Cl^-	HCO_3^-	Degree of mineralization
14800 mg/L	671.2 mg/L	5200 mg/L	14800 mg/L	800 mg/L	63863.2 mg/L	76 mg/L	100210 mg/L

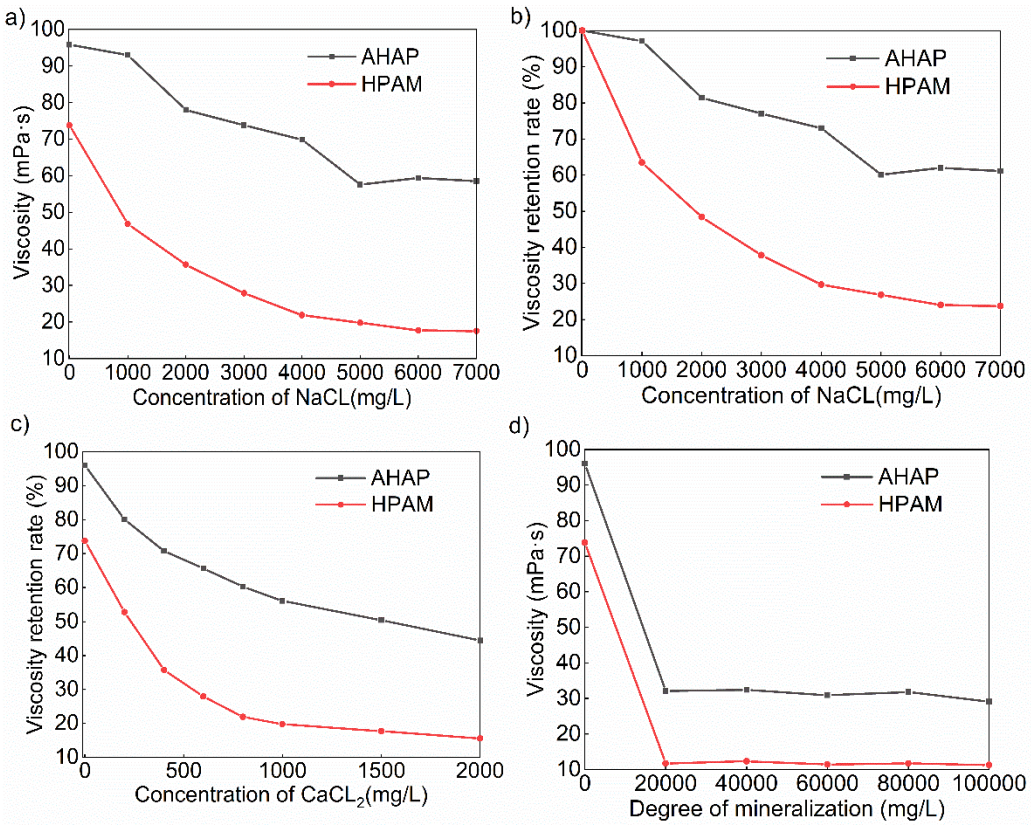


Fig. 12. Influence of different concentrations of inorganic salts on the apparent viscosity of polymer solution

The addition of salt affects polymer solution viscosity in two primary ways: (1) Charge Shielding Effect: Salt ions neutralize the charges on carboxylic acid groups in the polymer, weakening electrostatic repulsion between molecular chains. This causes the polymer chains to transition from an extended to a coiled conformation, reducing hydrodynamic volume and promoting intramolecular associations, thereby decreasing solution viscosity. (2) Enhanced Hydrophobic Associations: Salt increases solvent polarity, strengthening hydrophobic associations in the polymer. This facilitates intermolecular associations, leading to an increase in solution viscosity. HPAM lacks hydrophobic groups and relies solely on electrostatic shielding. Consequently, its salt resistance is poor, and its viscosity drops sharply with increasing salt concentration. In contrast, AHAP benefits from the competition between electrostatic shielding and enhanced hydrophobic associations, resulting in superior salt tolerance compared to conventional polymers.

In summary, AHAP solutions exhibit significantly higher viscosity retention rates than HPAM solutions in both monovalent (e.g., NaCl) and divalent (e.g., $CaCl_2$) salt environments, as well as in high-salinity complex brines. This demonstrates AHAP's excellent salt resistance.

3.8 Rheological performance evaluation

3.8.1 Temperature and shear resistance

Fig. 13 illustrates the viscosity changes of 0.6%, 0.5%, 0.4%, and 0.3% AHAP polymer fracturing fluids under shear at 170 s^{-1} while heating from 30°C to 60/80/100°C for 1 hour. The viscosity of the polymer solutions initially rises briefly before declining rapidly as temperature increases. This occurs because the hydrophobic association effect is temporarily enhanced when temperature begins to rise, leading to a short-term viscosity increase. However, when temperature exceeds a critical threshold, hydrophobic associations weaken, causing breakdown of crosslinking points and collapse of the three-dimensional network structure, ultimately reducing viscosity.

The inclusion of AMPS and DNS-86 in the AHAP polymer improves its thermal resistance. The bulky side groups in these components enhance the rigidity of the polymer chains, suppress hydrolysis of amide groups under high temperatures, and reduce the polymer's thermal sensitivity. Additionally, DNS-86 introduces hydrophobic associations that further enhance the fluid's thermal stability. Consequently, after 1 hour of shearing at 170 s^{-1} and 60/80/100°C, the viscosities of the polymer fluids at different concentrations remain at 96, 53, 60, and 50 mPa·s, respectively, all meeting industry standards (≥50 mPa·s). These results demonstrate that the AHAP polymer fracturing fluid exhibits excellent thermal and shear resistance,

maintaining stable viscosity even under high-temperature, high-shear conditions. By adjusting the thickener concentration based on field temperature requirements, the fluid can meet performance demands while reducing costs.

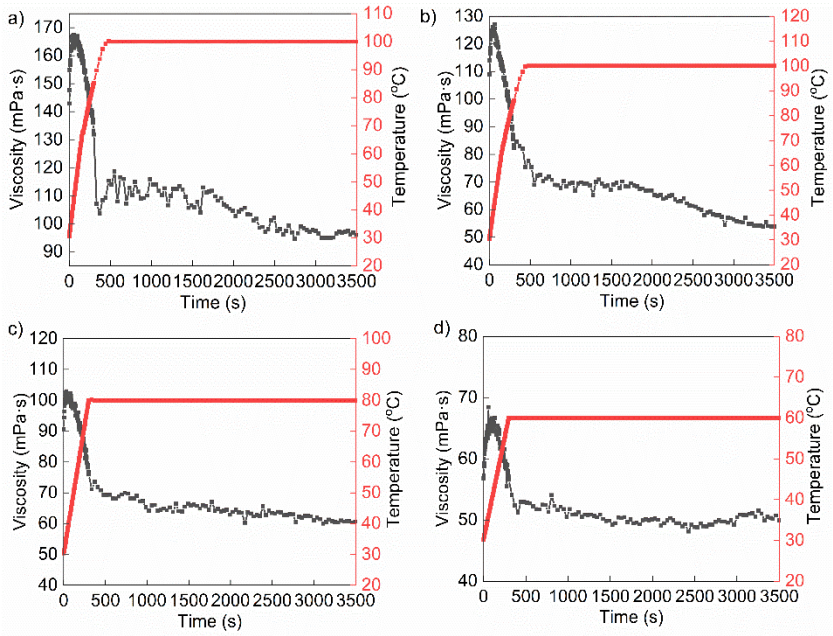


Fig. 13. Testing of temperature and shear resistance performance for polymer fracturing fluid systems (a 0.6%, b 0.5%, c 0.4%, d 0.3%)

3.8.2 Viscoelasticity

Traditionally, the apparent viscosity of fracturing fluids was considered a direct indicator of sand-carrying performance, with higher viscosity assumed to correlate with better proppant suspension. However, advancing theoretical research and experimental data have revealed that sand-carrying capacity is not governed by apparent viscosity

but rather by the elastic modulus (storage modulus, G') in viscoelastic properties, which dominates the dynamic suspension of proppants. Unlike conventional polymers, hydrophobically associating polymers (HAPs) form crosslinked network structures via hydrophobic interactions, endowing their solutions with superior viscoelasticity. In this study, the viscoelastic properties of AHAP polymer fracturing fluids—specifically, the storage modulus (G') and loss modulus (G")—were measured using a Haake rheometer. Fig. 14(a) presents stress sweep results for 0.3%, 0.4%, 0.5%, and 0.6% AHAP polymer fracturing fluids at 30 °C, a fixed frequency of 1.0 Hz, and a shear stress range of 0.01–35 Pa. As polymer concentration increases, the crossover point of G' and G" shifts to higher stresses, and the linear viscoelastic region expands. This indicates that higher-concentration fluids form denser internal network structures, enhancing elastic modulus (G') and structural strength. At a fixed frequency, greater stress is required to disrupt the network, shifting the yield point (G' = G") toward higher stress levels.

Fig. 14(b) shows frequency sweep results for the same AHAP concentrations at 30 °C, a fixed shear stress of 1.0 Pa, and a frequency range of 0.01–10 Hz. With increasing polymer concentration, the crossover point of G' and G" shifts to lower frequencies. This demonstrates that at fixed stress, the elastic-dominated regime (G' > G") occurs at lower frequencies for higher-concentration fluids. This behavior arises from the enhanced structural stability and prolonged relaxation time of concentrated solutions.

At low frequencies, the fluid has sufficient time to exhibit elastic responses, while viscous behavior dominates at high frequencies. Increased polymer concentration strengthens the network, extends relaxation times, and shifts the elastic-dominated regime to lower frequencies. These findings confirm the excellent viscoelasticity of AHAP polymer fracturing fluids, validating their superior sand-carrying capacity and suitability for field applications.

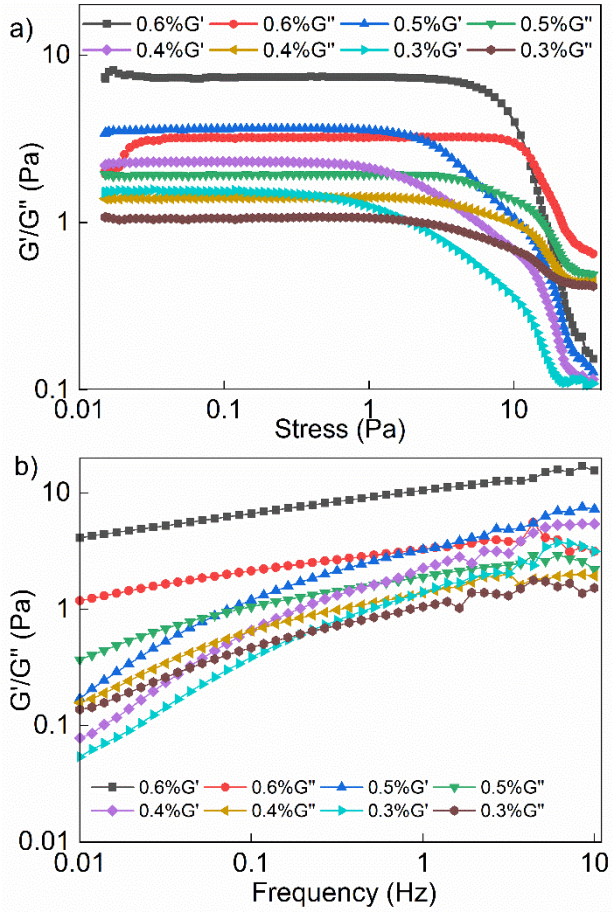


Fig. 14. The viscoelastic properties of polymer solutions with different concentrations. a) Stress scanning curve; b) Frequency scanning curve.

3.9 Sand carrying performance

Sand-carrying capacity refers to the ability of polymer fracturing fluids to suspend solid proppants such as quartz sand and ceramic particles. This property is typically evaluated by measuring the static settling rate of proppants in the fracturing fluid. The primary function of solid proppants is to provide effective stress support for fracture channels and maintain their flow conductivity. In fracturing operations, the sand-carrying performance of the fluid directly determines the success of the fracturing operation.

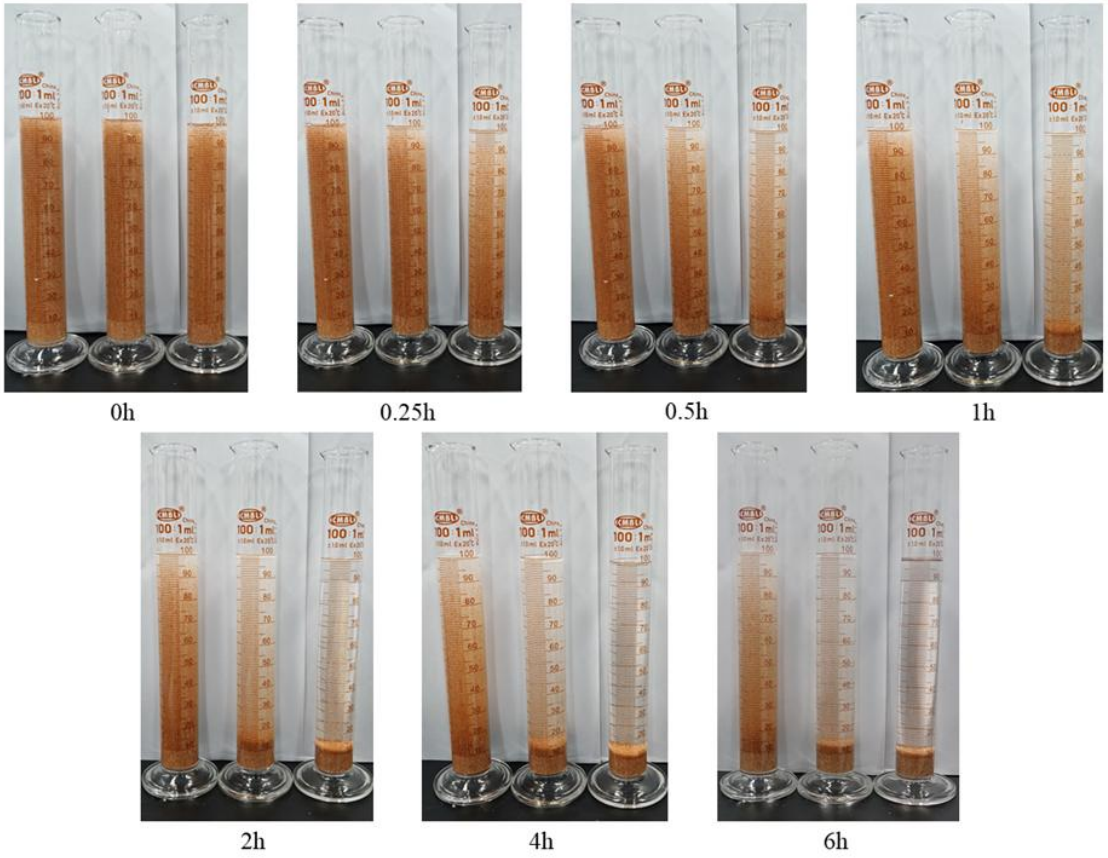
In this experiment, AHAP polymer fracturing fluids with concentrations of 0.5%, 0.4%, and 0.3% were prepared. Quartz sand (20–40 mesh) was added to the fluids at a sand ratio of 20%. The mixtures were maintained under static conditions at room temperature, with the initial position of the quartz sand recorded to observe static settling behavior. Results are shown in Table 2 and Fig. 15:

Table 2 Sand carrying performance of polymer fracturing fluids with different concentrations

Polymer concentration	Settling time /h	Settling distance /cm	Sedimentation rate /cm/min
0.3%	0.75	120	2.667
0.4%	2.25	120	0.889

0.5%	6	96	0.267

549



550

551 Fig. 15. Comparison of sand carrying performance of polymer fracturing fluids with different

552 concentrations

553 After 6 hours of natural settling in a 0.5% polymer fracturing fluid, a portion of quartz

554 sand remained suspended in the solution, with a settling rate of 0.263 cm/min. The

555 sand-carrying capacity of the polymer fracturing fluid system improves as polymer

556 concentration increases, as higher thickener dosage enhances the initial viscosity and

557 storage modulus of the fluid, resulting in superior sand suspension. Decades of

laboratory studies have established that a quartz sand settling rate of 0.08–0.18 mm/s (equivalent to 0.48–1.08 cm/min) in polymer fracturing fluids is considered optimal. The AHAP polymer fracturing fluid meets this requirement at concentrations of 0.4% and 0.5%. Considering that field conditions may introduce greater environmental variables compared to controlled lab settings, a 0.5% thickener concentration was selected for practical application. In summary, the AHAP polymer fracturing fluid exhibits excellent sand-carrying performance, fulfilling the requirements for field operations.

3.10 Breaker

After completing fracture creation and proppant placement, the polymer fracturing fluid must be hydrated and flowed back. The role of the gel breaker is to cleave polymer molecular chains, reducing fluid viscosity. Thus, the speed and completeness of gel breaking are critical to the success of fracturing operations.

In this experiment, AHAP polymer solutions (0.1%, 0.2%, 0.3%, 0.4%, 0.5%) and a 0.5% HPAM solution were prepared as fracturing fluids. Ammonium persulfate was added at varying concentrations as the gel breaker. The fluids were placed in a constant-temperature water bath at 80 °C to observe gel-breaking behavior, and the breaking time was recorded. After breaking, the solutions were cooled to room temperature, and

their surface/interfacial tensions were measured using a tension meter. The gel-breaking times and post-breakage tensions are summarized in Table 3:

Table 3 Comparison of rubber breaking properties of different polymer fracturing fluids

Dosage of thickening agent	Dosage of glue breaker	Breaking temperature /°C	Breaking time /min	Viscosity of breaking liquid /mPa·s	Surface tension /mN/m	Interfacial tension /mN/m
0.5%HPAM	0.03%		40	＜5	56.266	33.138
0.1%AHAP	0.01%		15	＜5	40.41	12.196
0.2%AHAP	0.01%		20	＜5	39.194	11.980
	0.01%		25	＜5	37.126	10.709
0.3%AHAP	0.02%		25	＜5	37.754	10.082
	0.03%	80	20	＜5	38.788	11.119
	0.01%		30	＜5	36.842	9.117
0.4%AHAP	0.02%		30	＜5	37.187	9.113
	0.03%		30	＜5	36.217	9.945
	0.01%		55	＜5	36.558	9.005
0.5%AHAP	0.02%		55	＜5	35.909	8.893
	0.03%		50	＜5	35.321	8.860

The AHAP polymer fracturing fluid systems at different concentrations could fully break within 1 hour under the action of gel breakers. The broken gel was clear and transparent with no residue, and no filament formation was observed when adhering to a glass rod. The viscosity of the broken gel, measured at 170 s^{-1} using a six-speed viscometer, was consistently below 5 mPa·s, confirming complete gel breaking. In addition to viscosity, the surface tension and interfacial tension of the broken gel are critical parameters. Lower surface and interfacial tensions of the broken gel reduce capillary retention effects, thereby mitigating water block damage and minimizing formation impairment. For aqueous fracturing fluids, industry standards typically require post-breakage surface tension ≤28.0 mN/m and interfacial tension (against kerosene) ≤2.0 mN/m. While the surface and interfacial tensions of the AHAP broken gel still deviate from these requirements (necessitating the addition of flowback aids to further reduce them), AHAP inherently exhibits better tension-lowering performance compared to HPAM. This advantage reduces the required dosage of flowback aids, thereby lowering operational costs. In summary, the AHAP fracturing fluid demonstrates excellent gel-breaking performance. With minor additions of flowback aids, it fully meets the field application requirements for fracturing fluids.

4 Conclusion

This experiment addresses the challenges of traditional polymer fracturing fluids in low-permeability reservoirs, such as poor temperature-salt resistance, inadequate gel-breaking efficiency, and high production costs, by designing and synthesizing a novel hydrophobic associative polymer fracturing fluid thickener, AHAP. Its performance was systematically evaluated. Using AM) the main chain monomer, AMPS, and an anionic hydrophobic monomer (DNS-86), AHAP was successfully synthesized via free radical polymerization in aqueous solution. The structure of the synthesized product was confirmed by FTIR and ^{1}H-NMR analysis. The polymer exhibited a molecular weight of approximately 1.13×10^{7} g/mol and excellent viscosity-enhancing capabilities. The experimental results show that AHAP fully dissolved in 870 s, slightly slower than HPAM (670 s), but the solution showed no residual flocs or aggregates, meeting field application requirements. AHAP solutions exhibited dual critical association concentrations (CAC): the first CAC at 0.085% and the second at 0.233%. Viscosity increased significantly above the second CAC, indicating effective formation of a 3D crosslinked network through hydrophobic association. Compared to HPAM, AHAP demonstrated superior temperature-salt resistance, as evidenced by viscosity stability under varying temperatures and single/composite saline conditions. Rheological tests confirmed that AHAP fracturing fluids maintained viscosities $\geq$ 50 mPa·s after shearing

616 at 170 s^{-1} and 60/80/100 ℃ for 1 h, demonstrating excellent temperature/shear
617 resistance. Adjusting thickener concentration based on field temperatures can optimize
618 performance and reduce costs. Storage modulus (G') and loss modulus (G") of AHAP
619 fracturing fluids met requirements across concentrations, ensuring suitability for field
620 operations. At 20% sand content, the settling rate of quartz sand in 0.5% AHAP fluid
621 was 0.267 cm/min, fulfilling empirical standards. Complete gel-breaking (< 5 mPa·s)
622 of 0.5% AHAP fluid occurred within 50 min using 0.03% ammonium persulfate. Post-
623 breakage surface tension and interfacial tension were 35.321 mN/m and 8.86 mN/m,
624 respectively. Although slightly exceeding industry standards, adding minimal flowback
625 aids can further optimize performance. In summary, AHAP shows excellent field
626 applicability and promising potential as a novel fracturing fluid thickener.
627

Funding Declaration:

This study was supported by the Strategic Cooperation Technology Projects of CNPC and CUPB (ZLZX2020-01).

References

[1] Y. Li, Y. Li, B. Wang, Z. Chen, D. Nie, The status quo review and suggested policies for shale gas development in China, Renewable and Sustainable Energy Reviews 59 (2016) 420-428, https://doi.org/10.1016/j.rser.2015.12.351 .

[2] H. Liao, H. Yu, G. Xu, P. Liu, Y. He, Y. Zhou, Polymer–Surfactant Flooding in Low-Permeability Reservoirs: An Experimental Study, ACS Omega 7(5) (2022) 4595-4605, https://doi.org/10.1021/acsomega.1c06582 .

[3] A. Das, N. Nguyen, Q.P. Nguyen, Low-tension gas process in high-salinity and low-permeability reservoirs, Petroleum Science 17(5) (2020) 1329-1344, https://doi.org/10.1007/s12182-020-00455-9 .

[4] A.C. Barbati, J. Desroches, A. Robisson, G.H. McKinley, Complex Fluids and Hydraulic Fracturing, Annual Review of Chemical and Biomolecular Engineering 7(Volume 7, 2016) (2016) 415-453, https://doi.org/10.1146/annurev-chembioeng-080615-033630 .

645 [5] S. Al-Hajri, B.M. Negash, M.M. Rahman, M. Haroun, T.M. Al-Shami, Perspective
646 Review of Polymers as Additives in Water-Based Fracturing Fluids, ACS Omega 7(9)
647 (2022) 7431-7443, https://doi.org/10.1021/acsomega.1c06739 .
648 [6] B. Zhang, B. Guo, G.a. Wu, S. Li, J. Shen, S. Xing, Y. Ying, X. Yang, X. Zhang,
649 M. Hu, J. Guo, Preparation of Temperature Resistant Terpolymer Fracturing Fluid
650 Thickener and Its Working Mechanism Study via Simulation Methods, Materials 18(5)
651 (2025) 1171, https://doi.org/10.3390/ma18051171 .
652 [7] J. Xu, H. Qin, H. Li, C. Lu, S. Li, D. Wu, Enhanced gas production efficiency of
653 class 1,2,3 hydrate reservoirs using hydraulic fracturing technique, Energy 263 (2023)
654 126003, https://doi.org/10.1016/j.energy.2022.126003 .
655 [8] J. Shi, Z. Wu, Q. Deng, L. Liu, X. Zhang, X. Wu, Y. Wang, Synthesis of
656 hydrophobically associating polymer: temperature resistance and salt tolerance
657 properties, Polymer Bulletin 79(7) (2022) 4581-4591, https://doi.org/10.1007/s00289-
658 021-03713-x .
659 [9] J. Mao, H. Tan, B. Yang, W. Zhang, X. Yang, Y. Zhang, H. Zhang, Novel
660 Hydrophobic Associating Polymer with Good Salt Tolerance, Polymers 10(8) (2018)
661 849, https://doi.org/10.3390/polym10080849 .
662 [10] H. Zheng, Y. Shi, Y. Tian, X. Yan, S. Zhao, R. Zhang, Synthesis and performance
663 evaluation of amphiphilic hyperbranched hydrophobically linked polymer thickeners,

664 Colloids and Surfaces A: Physicochemical and Engineering Aspects 715 (2025) 136667,
665 https://doi.org/10.1016/j.colsurfa.2025.136667 .
666 [11] G. Deng, R. Wang, G. Wang, Y. Jiao, Z. Wu, Y. Wei, W. Zhao, S. Chen, J. Zhong,
667 M. Zhou, Preparation and Evaluation of Salt-Resistant Hydrophobic Association
668 Polyacrylamide for Fracturing, ChemistrySelect 10(15) (2025) e202403999,
669 https://doi.org/10.1002/slct.202403999 .
670 [12] M.J. Rosen, Q. Zhou, Surfactant− surfactant interactions in mixed monolayer and
671 mixed micelle formation, Langmuir 17(12) (2001) 3532-3537,
672 https://doi.org/10.1021/la001197b .
673 [13] V. Patel, J. Trivedi, T. Sharma, Influence of hydrophobic association in the
674 aqueous media on the rheology and polymer conformation of associative polymers,
675 Polymer Bulletin 80(8) (2023) 8939-8959, https://doi.org/10.1007/s00289-022-04484-
676 9 .
677 [14] M. Nichifor, Role of Hydrophobic Associations in Self-Healing Hydrogels Based
678 on Amphiphilic Polysaccharides, Polymers 15(5) (2023) 1065,
679 https://doi.org/10.3390/polym15051065 .
680 [15] L. Wang, D. Wang, Y. Shen, X. Lai, X. Guo, Study on properties of hydrophobic
681 associating polymer as drag reduction agent for fracturing fluid, Journal of Polymer
682 Research 23(11) (2016) 1-8, https://doi.org/10.1007/s10965-016-1129-8 .

683 [16] Q. Zhao, L. Zhao, C. Ma, Synthesis and properties of fluorinated hydrophobic
684 association polyacrylamide as thickener for hydraulic fracturing fluid, Iranian Polymer
685 Journal 26(8) (2017) 589-595, https://doi.org/10.1007/s13726-017-0545-x .
686 [17] R. Yang, X. Lai, Q. Li, X. Ding, L. Wang, X. Wen, Y. Guo, Effect of hydrophobic
687 monomers with different carbon chains on the structure–activity relationship of
688 associating polyacrylamides, Journal of Polymer Research 31(8) (2024) 242,
689 https://doi.org/10.1007/s10965-024-04083-4 .
690 [18] Y. Zhang, E. Yan, Q. Chen, L. Zhao, Y. Wang, J. Deng, H. Zhang, H. Liu,
691 Influence of Alkyl Chain Length on the Performance of Inverse Emulsion
692 Polyacrylamide Fracturing Fluid Thickeners, Industrial & Engineering Chemistry
693 Research 63(13) (2024) 5513-5526, https://doi.org/10.1021/acs.iecr.3c04228 .
694 [19] X. Jing, Y. Liu, W. Zhao, J. Pu, Synthesis and drag reduction properties of a
695 hydrophobically associative polymer containing ultra-long side chains, BMC
696 Chemistry 17(1) (2023) 48, https://doi.org/10.1186/s13065-023-00968-5 .
697 [20] T. Liu, S. Gou, L. Zhou, J. Hao, Y. He, L. Liu, L. Tang, S. Fang, High-viscoelastic
698 graft modified chitosan hydrophobic association polymer for enhanced oil recovery,
699 Journal of Applied Polymer Science 138(11) (2021) 50004,
700 https://doi.org/10.1002/app.50004 .

701 [21] B.F. Abu-Sharkh, G.O. Yahaya, S.A. Ali, I.W. Kazi, Solution and interfacial
702 behavior of hydrophobically modified water-soluble block copolymers of acrylamide
703 and N-phenethylacrylamide, Journal of Applied Polymer Science 82(2) (2001) 467-476,
704 https://doi.org/10.1002/app.1873 .
705 [22] X. Qin, Q. Wang, P. Tang, H. Yang, C. Li, X. Yang, T. Peng, Synthesis,
706 Characterization, and Properties of a Novel Hyperbranched Polymers with
707 Polyacrylamide Side Chains, Materials 17(7) (2024) 1619,
708 https://doi.org/10.3390/ma17071619 .
709 [23] J.F. Argillier, A. Audibert, J. Lecourtier, M. Moan, L. Rousseau, Solution and
710 adsorption properties of hydrophobically associating water-soluble polyacrylamides,
711 Colloids and Surfaces A: Physicochemical and Engineering Aspects 113(3) (1996) 247-
712 257, https://doi.org/10.1016/0927-7757(96)03575-3 .
713 [24] Q. Wang, J. Mao, J. Zhao, H. Zhang, J. Xue, Q. Zhang, Y. Zhang, X. Yang, C. Lin,
714 J. Mao, Z. Huang, R. Peng, Synthesis of a salt-responsive hydrophobically associating
715 polymer for fracturing fluid based on self-assembling transition, Journal of Molecular
716 Liquids 366 (2022) 120201, https://doi.org/10.1016/j.molliq.2022.120201 .
717 [25] J. Li, Y.-X. Ji, X.-X. Ni, K.-H. Lv, X.-B. Huang, J.-S. Sun, A micro-crosslinked
718 amphoteric hydrophobic association copolymer as high temperature- and salt-resistance

719 fluid loss reducer for water-based drilling fluids, Petroleum Science 21(3) (2024) 1980-
720 1991, https://doi.org/10.1016/j.petsci.2024.01.021 .
721 [26] X. Li, C. Pan, H. Chen, Z. Zhang, K. Ning, Preparation and Performance
722 Evaluation of Temperature- and Salt-Resistant Hydrophobically Associated Polymer
723 Fracturing Fluids, ACS Omega 10(8) (2025) 8281-8291,
724 https://doi.org/10.1021/acsomega.4c10023 .
725 [27] Q. Zhang, J. Mao, Y. Liao, T. Xu, H. Zhang, A. Du, X. Yang, C. Lin, J. Mao,
726 Evaluation of temperature resistance of non chemical crosslinked double-tailed
727 hydrophobically associating polymer fracturing fluid, Reactive and Functional
728 Polymers 175 (2022) 105268, https://doi.org/10.1016/j.reactfunctpolym.2022.105268 .
729 [28] S. Zhu, M. Xu, S. Yang, Z. Huang, Y. Wang, Y. Zhu, Evaluation of shear resistance
730 of dendritic hydrophobic association polymers, Journal of Polymer Research 31(11)
731 (2024) 318, https://doi.org/10.1007/s10965-024-04177-z .
732 [29] H. Dai, Z. Huang, Y. Xiong, N. Chen, J. Lan, Z. He, S. Dai, D. Huang, Molecularly
733 designed nonionic hydrophobic association polymers with anti-salt capacity:
734 Enhancing drag reduction at high mineralization levels, Colloids and Surfaces A:
735 Physicochemical and Engineering Aspects 681 (2024) 132827,
736 https://doi.org/10.1016/j.colsurfa.2023.132827 .

[30] Z. Yang, M. Zhao, W. Bi, Y. Cheng, Z. Ma, K. Liu, Y. Li, C. Dai, Synthesis and analysis of drag reduction performance of the temperature-resistant polymer slickwater for high temperature reservoirs, Journal of Molecular Liquids 397 (2024) 124137, https://doi.org/10.1016/j.molliq.2024.124137 .

[31] Y. Du, Y. Zhu, Y. Ji, H. Xu, H. Zhang, S. Yuan, Effect of salt-resistant monomers on viscosity of modified polymers based on the hydrolyzed poly-acrylamide (HPAM): A molecular dynamics study, Journal of Molecular Liquids 325 (2021) 115161, https://doi.org/10.1016/j.molliq.2020.115161 .

[32] S. Liu, X. Wu, H. Liu, P. Zhou, Z. Tang, J. Zhang, M. Li, Synthesis of suspension stabilizers for isolation fluids by response surface methodology and study of their properties, Colloids and Surfaces A: Physicochemical and Engineering Aspects 702(2) (2024) 135139, https://doi.org/10.1016/j.colsurfa.2024.135139 .

[33] Jorgensen, W. L.; Maxwell, D. S.; Tirado-Rives, J., Development and Testing of the OPLS All-Atom Force Field on Conformational Energetics and Properties of Organic Liquids. Journal of the American Chemical Society 1996, 118 (45), 11225-11236.

[34] Abdel-Azeim, S.; Kanj, M. Y., Dynamics, Aggregation, and Interfacial Properties of the Partially Hydrolyzed Polyacrylamide Polymer for Enhanced Oil Recovery

755 Applications: Insights from Molecular Dynamics Simulations. Energy & Fuels 2018,
756 32 (3), 3335-3343.
757 [35] Lu, T., A comprehensive electron wavefunction analysis toolbox for chemists,
758 Multiwfn. The Journal of Chemical Physics 2024, 161 (8).
759 [36] Lu, T.; Chen, F., Multiwfn: A multifunctional wavefunction analyzer. Journal of
760 Computational Chemistry 2012, 33 (5), 580-592.
761 [37] Darden, T.; York, D.; Pedersen, L., Particle mesh Ewald: An N · log(N) method for
762 Ewald sums in large systems. The Journal of Chemical Physics 1993, 98 (12), 10089-
763 10092.
764 [38] Hess, B.; Bekker, H.; Berendsen, H. J. C.; Fraaije, J. G. E. M., LINCS: A linear
765 constraint solver for molecular simulations. Journal of Computational Chemistry 1997,
766 18.
767 [39] Lemak, A. S.; Balabaev, N. K., On The Berendsen Thermostat. Molecular
768 Simulation 1994, 13 (3), 177-187.
769 [40] Martoňák, R.; Laio, A.; Parrinello, M., Predicting Crystal Structures: The
770 Parrinello-Rahman Method Revisited. Physical Review Letters 2003, 90 (7), 075503.
771 [41] Humphrey, W.; Dalke, A.; Schulten, K., VMD: Visual molecular dynamics.
772 Journal of Molecular Graphics 1996, 14 (1), 33-38.

773 [42] Quezada, G. R.; Saavedra, J. H.; Rozas, R. E.; Toledo, P. G., Molecular dynamics
774 simulations of the conformation and diffusion of partially hydrolyzed polyacrylamide
775 in highly saline solutions. Chemical Engineering Science 2020, 214, 115366.
776 [43] Martínez, L.; Andrade, R.; Birgin, E. G.; Martínez, J. M., PACKMOL: A package
777 for building initial configurations for molecular dynamics simulations. Journal of
778 Computational Chemistry 2009, 30 (13), 2157-2164.
779
780